Commun Nonlinear Sci Numer Simulat 96 (2021) 105689

Contents lists available at ScienceDirect

Commun Nonlinear Sci Numer Simulat

journal homepage: www.elsevier.com/locate/cnsns

Research paper

Short-term and spike-timing-dependent plasticity facilitate the formation of modular neural networks

Ewandson L. Lameu[a], Fernando S. Borges[b], Kelly C. Iarosz[c], Paulo R. Protachevicz[c], Chris G. Antonopoulos[d], Elbert E.N. Macau[a,e], Antonio M. Batista[c,f,*]

[a] National Institute for Space Research, São José dos Campos, São Paulo, 12227-010, Brazil
[b] Center for Mathematics, Computation and Cognition, Federal University of ABC, São Bernardo do Campo, São Paulo, 09606-045, Brazil
[c] Institute of Physics, University of São Paulo, São Paulo, 05508-900, Brazil
[d] Department of Mathematical Sciences, University of Essex, Wivenhoe Park, UK
[e] Federal University of São Paulo, São José dos Campos, São Paulo, 12247-014, Brazil
[f] Department of Mathematics and Statistics, State University of Ponta Grossa, Ponta Grossa, Paraná, 84030-900, Brazil

ARTICLE INFO

Article history:
Received 22 July 2020
Revised 10 November 2020
Accepted 27 December 2020
Available online 29 December 2020

Keywords:
short-term plasticity
spike-time dependent plasticity
modular networks

ABSTRACT

The brain has the phenomenal ability to reorganise itself by forming new connections among neurons and by pruning others. The so-called neural or brain plasticity facilitates the modification of brain structure and function over different time scales. Plasticity might occur due to external stimuli received from the environment, during recovery from brain injury, or due to modifications within the body and brain itself. In this paper, we study the combined effect of short-term (STP) and spike-timing-dependent plasticity (STDP) on the synaptic strength of excitatory coupled Hodgkin-Huxley neurons and show that plasticity can facilitate the formation of modular neural networks with complex topologies that resemble those of networks with preferential attachment properties. In particular, we use an STDP rule that alters the synaptic coupling intensity based on time intervals between spikes of postsynaptic and presynaptic neurons. Previous work has shown that STDP may induce the emergence of directed connections from high to low frequency spiking neurons. On the other hand, STP is attributed to the release of neurotransmitters in the synaptic cleft of neurons that alter its synaptic efficiency. Our results suggest that the combined effect of STP and STDP with long recovery times facilitates the formation of connections among neurons with similar spike frequencies only, a kind of preferential attachment. We then pursue this further and show that, when starting with all-to-all neural configurations, depending on the STP recovery time and distribution of neural frequencies, modular neural networks can emerge as a direct result of the combined effect of STP and STDP.

1. Introduction

Mathematical models have been employed in neuroscience since early in the 20th century [1] to explain experimental findings and elucidate the inner workings of the brain. In 1907, Lapicque [2] proposed the integrate-and-fire model that can

* Corresponding author at: Department of Mathematics and Statistics, State University of Ponta Grossa, Ponta Grossa, Paraná, 84030-900, Brazil.
E-mail address: abatista@uepg.br (A.M. Batista).

https://doi.org/10.1016/j.cnsns.2020.105689
1007-5704/

reproduce the electrical activity of the membrane potential of neurons. It is one of the most popular models for studying the dynamic behaviour of neural systems. Later in 1952, Hodgkin and Huxley [3] explained the ionic mechanisms in the cell membrane of neurons and proposed the so-called Hodgkin-Huxley (HH) neural model that has, since then, been used extensively to study neural networks [4].

In particular, neural network models have been used extensively in computational neuroscience, such as in studies of neural dynamics [5], dynamic range [6–9], neural synchronisation [10–14], flow of information [15–17], and brain plasticity [18,19] to name a few.

Neural plasticity is the ability of the brain to modify its function and structure over different time scales [21,22]. The term was initially used by James [23] in 1890 to propose that phenomena of habit in living organisms are due to plasticity. Cajal [24] reported in the early 1900s his research about regenerative and degeneration changes in brain structure. In 1924, Lashley [25] demonstrated experimental evidence of a malleable brain. Konorski [26] and Hebb [27] proposed in 1948 and 1949, respectively, that neural activities influence the connection among neurons. In 1960, Bennet et al. [28] carried out experiments with rats and observed chemical and anatomical plasticity in the brain. Since then, there have been many theoretical [29] and empirical [30] studies aiming to explain and understand brain plasticity and its effects in brain structure and function.

In synaptic plasticity, the synapses among neurons are potentiated or depressed in time according to the activity of other neurons [31,32]. Recent works [33,34] have shown that short-term (STP) and spike-timing-dependent plasticity (STDP) are different forms of neural processes leading to synaptic modifications. In particular, STDP depends on the relative timing of presynaptic and postsynaptic neural spikes [35,36]. This type of plasticity can lead to various dynamical phenomena and coupling structures, such as stable localised structures [37], stimulation-induced synchronisation or desynchronisation [38], noise-enhanced synchronisation [39,40] and nontrivial topology [20]. The STDP mechanism plays a role in temporal coding of information by spikes [37,41]. On the other hand, STP is attributed to the release of neurotransmitters in the synaptic cleft of neurons that alter its synaptic efficiency and acts on shorter time scales, ranging from milliseconds to hundreds to thousands of milliseconds [42–45]. As in the case with STDP, STP influence significantly the dynamical behaviour in a network. For instance, it may stabilise the parametric working memory [46], contribute to the emergence of spontaneous travelling waves [47], or induce phase changes in neural postsynaptic spiking [33].

Here, we extend the work in Borges et al. [20] which was focused on STDP only and study the combined effect of STP and STDP in neural networks of excitatory coupled HH neurons. The plasticity terms that model STDP in the equations in Section 2 are based on the experimental results by Bi and Poo [48,49] that were performed on excitatory synapses and on theoretical results by Abbott et al. [43] and Popovych et al. [39] (STDP). The results in Bi and Poo [48,49] show that STDP is a function of the relative timing of postsynaptic and presynaptic spikes and is theoretically backed by the Hebbian synaptic learning rule [27]. Instead, STP depends on the neural recovery dynamics [50,51]. McDonnell and Graham [33] used mathematical analysis and numerical simulations to show that STP induces phase changes in neural postsynaptic spiking. In our work, we start by studying the simplest case of a pair of HH neurons for a range of spike frequencies, aiming to understand how connectivity between them changes by the combined effect of STP and STDP. Next, we build an initially, all-to-all (globally) connected network of HH neurons and consider the simultaneous effect of STP and STDP for a range of coupling strengths. We show that STP plays an important role in changes of connectivity in neural networks with STDP. Indeed, we find that for high STP recovery time, only neurons with similar spike frequencies tend to connect, a form of preferential attachment. More importantly, our results show that, when starting with all-to-all networks, depending on the STP recovery time and distribution of neural frequencies, modular neural networks can emerge as a direct result of the combined effect of STP and STDP, a structure depicted by neurophysiological and experimental studies [52,53]. For the considered setup, STP plays a balancing role: while STDP tends to synchronise all neurons in a cluster, STP destroys the strong synchronisation and leads to a modular structure.

The paper is organised as follows: In Section 2, we introduce the general mathematical model of HH neural networks with STP and STDP and, in Section 3, we present our analysis and results based on numerical simulations, that show the effects of both types plasticity, initially on a pair of neurons and then, on a network of 100 HH neurons. Finally, we present the conclusions of our work in the last section.

2. A Hodgkin-Huxley neural network with STP and STDP

In our work, we build use a neural network model of N HH neurons coupled with excitatory chemical synapses, equipped with STP and STDP rules based on experimental results in Bi and Poo [48,49] and on theoretical models proposed by Popovych et al. [39] (STDP) and McDonnell and Graham [33,43,50] (STP).

Specifically, the HH neural network model considered here is given by

$$\begin{aligned} C\dot{V}_i = {} & I_i - g_{\mathrm{K}} n_i^4 (V_i - E_{\mathrm{K}}) g_{\mathrm{Na}} m_i^3 h_i (V_i - E_{\mathrm{Na}}) \\ & - g_L (V_i - E_{\mathrm{L}}) + (V_r - V_i) \sum_{j=1}^{N} \varepsilon_{ij} f_j D_j, \end{aligned} \tag{1}$$

$$\dot{n}_i = \alpha_{n_i}(V_i)(1 - n_i) - \beta_{n_i}(V_i) n_i, \tag{2}$$

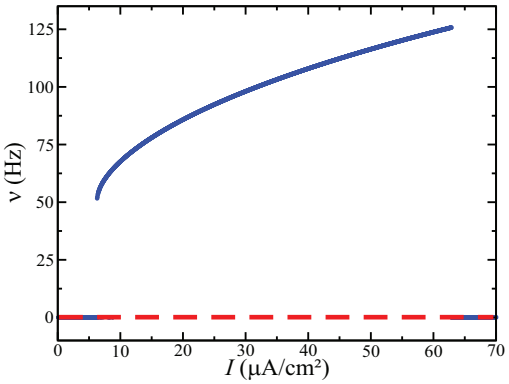

Fig. 1. Natural frequency ν as a function of the current I for a single HH neuron.

$$\dot{m}_i = \alpha_{m_i}(V_i)(1 - m_i) - \beta_{m_i}(V_i)m_i, \tag{3}$$

$$\dot{h}_i = \alpha_{h_i}(V_i)(1 - h_i) - \beta_{h_i}(V_i)h_i, \tag{4}$$

$$\dot{f}_i = -\frac{f_i}{\tau_s}, \tag{5}$$

$$\dot{D}_i = \frac{1 - D_i}{\tau_D}, \tag{6}$$

where C (in μF/cm^2) is the membrane capacitance and V_i (in mV) the membrane potential of neuron i at time t, with $i = 1, \ldots, N$. I_i (in μA/cm^2) is the constant current density of neuron i and ε_{ij} represents the matrix of coupling weights between neurons i and j. Parameters n_i and m_i are the activation of potassium and sodium functions, respectively, and h_i the inactivation of sodium function. Parameters g and E are associated with the conductance and reversal potential of each ion, respectively, and V_r is the excitatory reversal potential.

The various rate functions in Eqs. (1)–(6) are given by

$$\alpha_n(V) = \frac{0.01V + 0.55}{1 - \exp(-0.1V - 5.5)}, \tag{7}$$

$$\beta_n(V) = 0.125 \exp\left(\frac{-V - 65}{80}\right), \tag{8}$$

$$\alpha_m(V) = \frac{0.1V + 4}{1 - \exp(-0.1V - 4)}, \tag{9}$$

$$\beta_m(V) = 4 \exp\left(\frac{-V - 65}{18}\right), \tag{10}$$

$$\alpha_h(V) = 0.07 \exp\left(\frac{-V - 65}{20}\right), \tag{11}$$

$$\beta_h(V) = \frac{1}{1 + \exp(-0.1V - 3.5)}, \tag{12}$$

We consider $C = 1$ μF/cm^2, $g_K = 36$ mS/cm^2, $g_{Na} = 120$ mS/cm^2, $g_L = 0.3$ mS/cm^2, $E_K = -77$ mV, $E_{Na} = 50$ mV, $E_L = -54.4$ mV and $V_r = 20$ mV.

Fig. 1 shows the spike (or natural) frequency ν (Hz) of a single HH neuron as a function of current I. The spikes were numerically computed when the voltage V crosses the threshold of 0mV, increasing from negative to positive values. In the simulations of 100 coupled HH neurons in Section 4, we consider I_i randomly distributed in the interval [10,30] μA/cm^2,

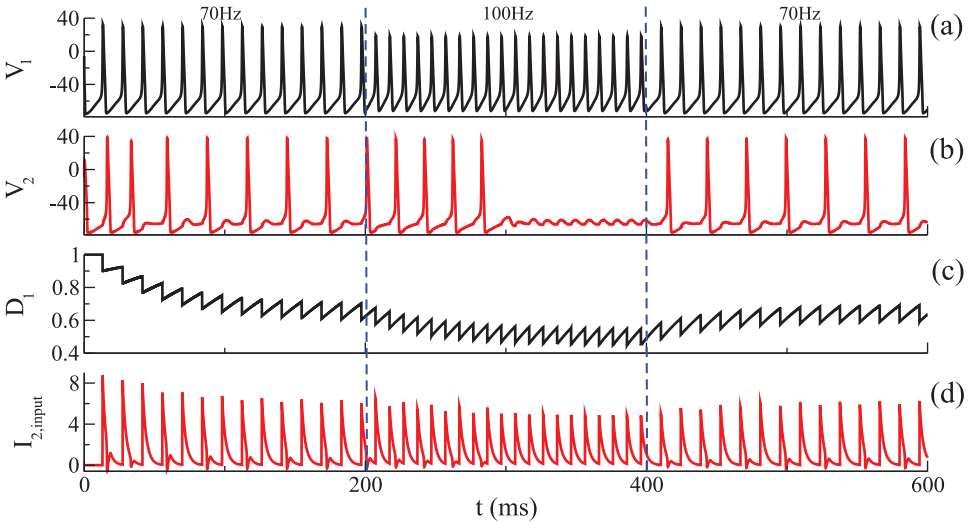

Fig. 2. The effect of STP on a pair of unidirectionally connected HH neurons, where neuron 1 is connected to neuron 2 but not vice versa: Temporal evolution of (a) V_1, (b) V_2, (c) D_1 and (d) $I_{2,\text{input}} = (V_r - v_2)\varepsilon_{21} f_1 D_1$ with $\varepsilon_{12} = 0$, $\varepsilon_{21} = 0.1$, $I_2 = 0$ and $\tau_D = 50$ ms. Note that, for $\nu_1 = 70$ Hz and $\nu_1 = 100$ Hz, we used $I_1 = 10.97$ μA/cm^2 and $I_1 = 31.8$ μA/cm^2, respectively.

leading to spike frequencies ν_i in the interval [70,100] Hz. This choice of interval also allows for the monotonic increase of the natural frequencies ν_i without reaching currents I bigger than 60 μA/cm^2 that correspond to a non-spike regime.

In Eq. (5), f_i is the strength of the effective synaptic output current from neuron i to neuron j and τ_s (in ms) the synaptic time constant, fixed at $\tau_s = 2.728$ ms. When neuron i spikes, f_i is updated ($f_i \to 1$) before it starts to decay exponentially.

Eq. (6) models STP [33,50] with τ_D (in ms) being the recovery time constant, related to biological mechanisms such as the depletion of release-ready neurotransmitter vesicles at the presynaptic terminal [44,51]. We assume that every time neuron i spikes, the update rule $D_i \to D_i - d$ is applied. Biologically, D_i could represent the vesicles that can be used to transmit a signal from the presynaptic to the postsynaptic neuron. Therefore, the update rule means that the amount D_i of available vesicles is decreased by $d = 0.1$ at every spike of neuron i, and then it recovers according to Eq. (6). We verify that different values of d lead qualitatively to the same behaviour. In that framework, D_i lies in [0,1] as if it happens D_i to be negative, it means that the neuron used all stored vesicles and when this happens, D_i is reset to 0. On the other hand, when D_i is equal to 1, it means that all neurotransmitter vesicles are restored.

Fig. 2 shows the effect of STP on a pair of neurons coupled with a unidirectional connection from neuron 1 to neuron 2. This is implemented by fixing $\varepsilon_{12} = 0$ (i.e. the connectivity strength from neuron 2 to neuron 1 is 0) and $\varepsilon_{21} = 0.1$ for the connectivity strength from neuron 1 to 2. In this study, we have set the STP recovery time τ_D at 50 ms and I_2 at 0, so that neuron 2 spikes only when it receives a strong enough input $I_{2,\text{input}} = (V_r - V_2)\varepsilon_{21} f_1 D_1$ from neuron 1. When the spiking frequency ν_1 in Fig. 2(a) changes from 70 Hz to 100 Hz, ν_2 in Fig. 2(b) exhibits a delayed alteration in its dynamic behaviour as its amplitude plummets at about 300 ms. We investigate further this phenomenon through the temporal evolution of D_1 in Fig. 2(c) and the input current $I_{2,\text{input}}$ received by neuron 2 in Fig. 2(d). Comparing the 70 Hz-regime with the 100 Hz-regime in Fig. 2(c) and (d), one can see that D_1 decreases with the increase of the spike-frequency of neuron 1 to 100 Hz, and consequently $I_{2,\text{input}}$ becomes less intense as it is not strong enough to cause spikes in the activity of neuron 2. When neuron 1 returns to 70 Hz spike frequency, there is more time for D_1 to recover, thereby to increase the intensity of $I_{2,\text{input}}$, which triggers again spikes in the activity of neuron 2. Generalising this, one might say that STP increases the variability of postsynaptic responses to presynaptic frequency changes.

Moving now to the other form of plasticity introduced to the model, STDP gives rise to changes in the synaptic strength by means of the update function [39,48]

$$\varepsilon_{ij} \to \varepsilon_{ij} + 10^{-3}\Delta\varepsilon_{ij}, \tag{13}$$

where

$$\Delta\varepsilon_{ij} = \begin{cases} \varepsilon_+ = A_1 e^{(-\Delta t_{ij}/\tau_1)}, & \text{if} \quad \Delta t_{ij} > 0 \\ \varepsilon_- = -A_2 e^{(\Delta t_{ij}/\tau_2)}, & \text{if} \quad \Delta t_{ij} < 0. \\ 0, & \text{if} \quad \Delta t_{ij} = 0 \end{cases}$$

Here, $\Delta t_{ij} = t_i - t_j$ is the time difference between the spike time t_i of the postsynaptic neuron i and the time t_j of the presynaptic neuron j, where $t_i > t_j$, leading to $\Delta t_{ij} > 0$. Fig. 3 shows the plot of the plasticity function $\Delta\varepsilon_{ij}$ calculated from Eq. (14) for $A_1 = 1$, $A_2 = 0.5$, $\tau_1 = 1.8$ ms, $\tau_2 = 6$ ms, and Δt_{ij} varying from -20 ms to 20 ms. This update rule is applied every time the postsynaptic neuron i spikes.

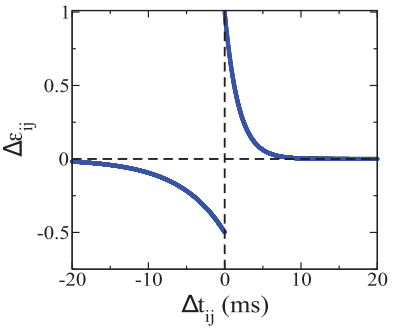

Fig. 3. Plot of $\Delta\varepsilon_{ij}$ that models STDP as a function of the difference between the spike times of the postsynaptic neuron i and presynaptic neuron j. Note the discontinuity at $\Delta t_{ij} = 0$ ms.

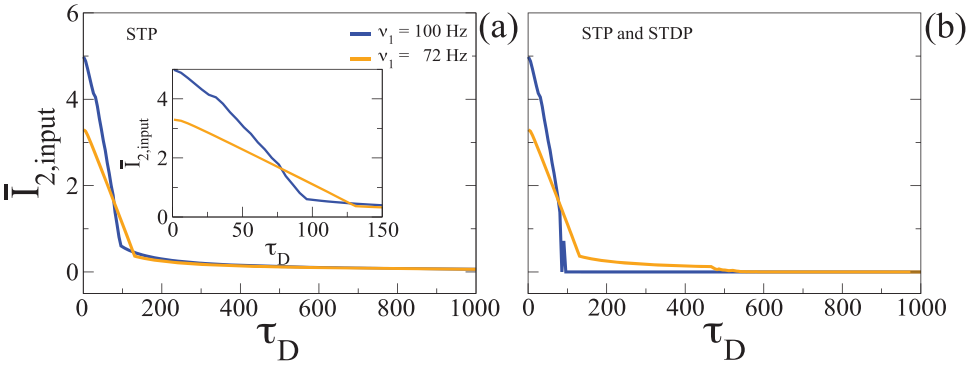

Fig. 4. The average input current $\bar{I}_{2,input}$ neuron 2 receives from neuron 1 as a function of the recovery time τ_D for the following cases: (a) only STP and (b) STP and STDP. Neuron 2 has a fixed spike frequency $\nu_2 = 70$ Hz ($I_2 = 10.97$ μA/cm^2). The blue curve represents the case where $\nu_1 = 100$ Hz ($I_1 = 31.8$ μA/cm^2) and the orange curve, the case where $\nu_1 = 72$ Hz ($I_1 = 11.88$ μA/cm^2). We use $\varepsilon_{21} = 0.3$ and $\varepsilon_{12} = 0$, to implement the case where ε_{21} changes when STDP is considered. Note that the simulations run for 200×10^3 ms and that $\bar{I}_{2,input}$ was calculated over the last 10×10^3 ms.

To understand better the effects of the recovery time τ_D, we consider in the next the case of two, unidirectionally connected neurons where neuron 1 (presynaptic) is connected to neuron 2 (postsynaptic), but not vice versa. We evaluate how the average input current $\bar{I}_{2,input}$ change with the increase of the recovery time τ_D by comparing cases where the neurons have similar and dissimilar spike frequencies.

Specifically, we consider the cases where the system is equipped with only STP (see Fig. 4(a)) and, STP and STDP (see Fig. 4(b)). In both cases, we consider $\varepsilon_{21} = 0.3$ and $\varepsilon_{12} = 0$, but for the case of STD and STDP (Fig. 4(b)), STDP acts only on ε_{21} (unidirectional connection) ensuring that the spike frequency of presynaptic neuron 1 remains unchanged. The spike frequency of neuron 2 was fixed at $\nu_2 = 70$ Hz ($I_2 = 10.97$ μA/cm^2) and, for the blue curves in Fig. 4, neuron 1 has $\nu_1 =$ 100 Hz ($I_1 = 31.8$ μA/cm^2) and for the orange curves, $\nu_1 = 72$ Hz ($I_1 = 11.88$ μA/cm^2). For the calculation of $\bar{I}_{2,input}$, we consider the last 10×10^3 ms of the simulations.

Observing Fig. 4(a) (STP), one can see that for recovery times $\tau_D < 75$ ms, the average current $\bar{I}_{2,input}$ for $\nu_1 = 100$ Hz (blue curve) is bigger than $\bar{I}_{2,input}$ for $\nu_1 = 72$ Hz (orange curve) (see also the inset in Fig. 4(a)). Interestingly, this change in the region 75 ms$< \tau_D <$ 125 ms where $\bar{I}_{2,input}$ for $\nu_1 = 72$ Hz (orange curve) is bigger than $\bar{I}_{2,input}$ for $\nu_1 = 100$ Hz (blue curve). For $\tau_D > 125$ ms, both $\bar{I}_{2,input}$ curves assume similar values and settle asymptotically to zero with further increasing in τ_D. In Fig. 4(b) (STP and STDP), we see that the action of STP and STDP causes $\bar{I}_{2,input}$ for $\nu_1 = 100$ Hz to drop to 0 at $\tau_D \approx 100$ ms, whereas $\bar{I}_{2,input}$ for $\nu_1 = 72$ Hz (orange curve) stays positive until $\tau_D \approx 480$ ms.

These results show that STP make the influence of slower (or close frequency) neurons to become greater than that of faster (or very different frequency) neurons as τ_D increases. In conjunction with STDP, this effect occurs due to the decrease of $\bar{I}_{2,input}$ that makes the firing times uncorrelated (less synchronised), which then causes the coupling to disappear, i.e. $\varepsilon_{21} \to 0$. This decoupling process tends to occur for smaller τ_D values as the difference between ν_1 and ν_2 is amplified. We address this further later when we discuss the results in Fig. 5.

3. Two HH neurons case

Neural networks with STDP and random synaptic input were studied by Popovych et al. [39]. The authors reported that the mean synaptic coupling depends on noise intensity. Recently, the authors in [20] showed that STDP induces non-trivial

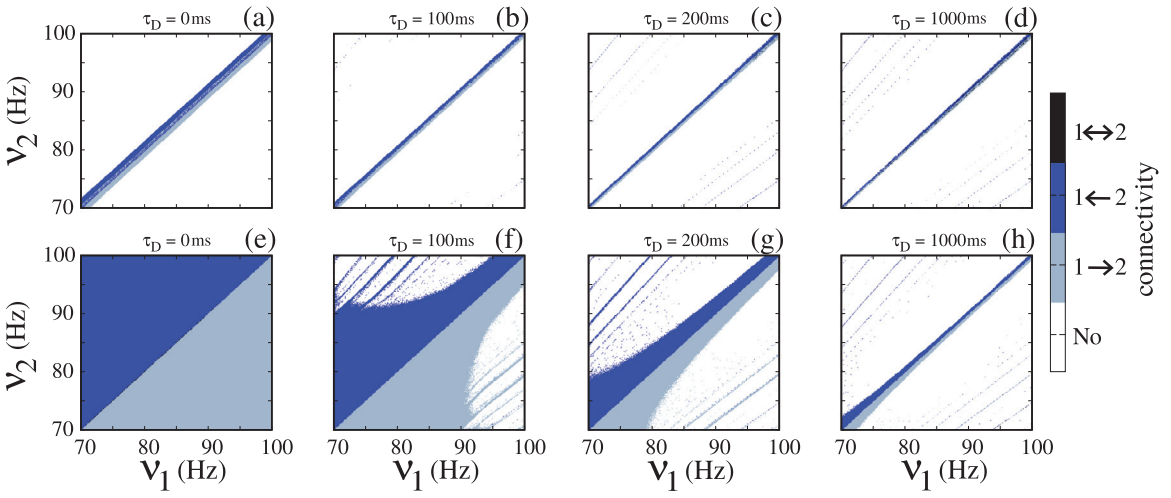

Fig. 5. Parameter spaces $\nu_1 \times \nu_2$ for a pair of initially uncoupled neurons for recovery times (a) $\tau_D = 0$ ms, (b) $\tau_D = 100$ ms, (c) $\tau_D = 200$ ms and (d) $\tau_D = 1000$ ms, and for a pair of initially coupled neurons for (e) $\tau_D = 0$ ms, (f) $\tau_D = 100$ ms, (g) $\tau_D = 200$ ms and (h) $\tau_D = 1000$ ms. Note that ν_1 and ν_2 vary in [70,100] Hz and that the colour bar shows the direction of synaptic connectivity, where white accounts for the uncoupled case (denoted "No"), grey for the case where neuron 1 is connected to neuron 2 (i.e. $1 \rightarrow 2$), blue for the case where neuron 2 is connected to neuron 1 (i.e. $1 \leftarrow 2$) and black for the bidirectional connection (i.e. $1 \leftrightarrow 2$).

topology in neural networks. Here, we extend this work and build a neural network of $N = 100$ HH neurons to study the combined effect of STP and STDP on the structure of the network and in particular, on its connectivity.

We start by analysing neural connectivity under the effect of STP and STDP. To this end, we consider a pair of HH neurons with STP and STDP, with the coupling strengths ε_{12} and ε_{21} varying in [0,0.3], and the connectivity threshold set at 0.01. This threshold is chosen because the coupling weights that should vanish in time actually oscillate around 0 assuming very small values as STDP is always present and thus, affecting them. As a consequence, the time averages of the coupling weights are not 0 but very close to 0. Moreover, for coupling weights smaller than this threshold, we notice that neurons influence each other only slightly.

Initially, the pair of neurons is uncoupled (i.e. $\varepsilon_{12} = \varepsilon_{21} = 0$) or bidirectionally coupled with $\varepsilon_{12} = \varepsilon_{21} = 0.3$. Fig. 5 shows the direction of connectivity, after a transient time, for different natural frequencies ν_1 and ν_2 in $[70, 100]$ Hz. The direction is coloured according to the connection from the output of one neuron to the input to the other neuron (directions of arrows in the colour bar): white accounts for the uncoupled case denoted in the colour bar as "No" ($\bar{\varepsilon}_{ij} < 0.01$), grey for the case where neuron 1 is connected to neuron 2 (i.e. $1 \rightarrow 2$), blue for the case where neuron 2 is connected to neuron 1 (i.e. $1 \leftarrow 2$), and black for the bidirectional connection (i.e. $1 \leftrightarrow 2$). For initially uncoupled neurons, the connections remain only for neurons with very similar frequencies, from those with faster spike frequencies to those with slower, as depicted in Fig. 5(a) ($\tau_D = 0$ ms), Fig. 5(b) ($\tau_D = 100$ ms), Fig. 5(c) ($\tau_D = 200$ ms) and Fig. 5(d) ($\tau_D = 1000$ ms). We note the absence of bidirectional connections and that the increase of the recovery time τ_D gives rise to a narrower region of directed connections. With regard to neurons starting with bidirectional connections, we observe that for $\tau_D = 0$ ms, neurons still remain unidirectionally connected (for all natural frequencies) from the high to the low frequency neurons (see Fig. 5(e)). Increasing τ_D to 100 ms (see Fig. 5(f)), 200 ms (Fig. 5(g)) and 1000 ms (Fig. 5(h)), we observe a decrease in the area that represents connectivity, implying that the region of high spike frequencies is more affected by the influence of STP. Therefore, STDP makes the connections increase from faster spiking to slower spiking neurons and STP decreases the influence of high frequency neurons, allowing connections only for those neurons with similar spike frequencies.

The reason for the initially, bidirectionally coupled system to have larger areas of connectivity is related to the difference in frequency $\Delta\nu_{ij}^c$ of neurons when coupled (or the synchronisation level). We note that this difference is not equal to the difference between their natural frequencies $\nu_i - \nu_j$, i.e. $\Delta\nu_{ij}^c \neq \nu_i - \nu_j$. In Fig. 6, we present the calculation of the average $\Delta\nu_{ij}^c$ (colour bar) for the first $t = 4000$ ms for the system with STP only. We consider $N = 2$, $\varepsilon_{12} = \varepsilon_{21} = 0.3$ and vary ν_1 and ν_2 in [70,100] Hz. Fig. 6(a) shows the result for $\tau_D = 0$ ms where, despite the natural frequencies of the neurons, $\Delta\nu_{ij}^c$ is approximately equal to 0 (black region). When comparing these results with the results in Fig. 5(e), once can see that this corresponds to a connected region. For increasingly bigger recovery times τ_D (see Fig. 6(b) for $\tau_D = 100$ ms, Fig. 6(c) for $\tau_D = 200$ ms and Fig. 6(d) for $\tau_D = 1000$ ms), one can observe a decrease in the size of the black area, similar to the size of the area seen in Fig. 5(f), (g) and (h). Thus, one can infer that what defines a connected configuration in the case of STDP is the difference in spike frequency among neurons or how synchronised they become. The non-homogeneous distribution of connected areas in relation to the main diagonal in Fig. 5 occurs due to the non-linear variation of neural frequencies in relation to the received external current. In Fig. 1, we see that for low currents (i.e. $I \in [10, 25]$), a small increase in I can cause a bigger variation in the frequencies when compared to the interval where $I > 30$. Therefore, low frequency

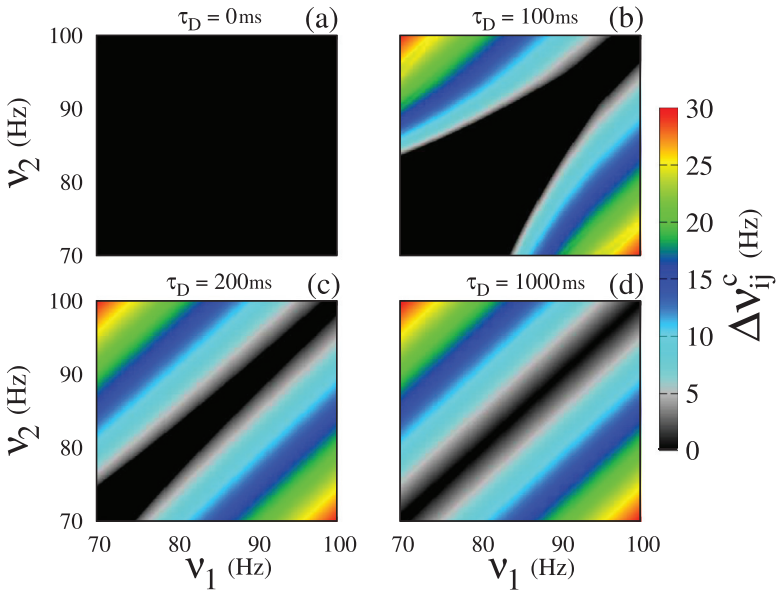

Fig. 6. Parameter space $\nu_1 \times \nu_2$ for increasing values of τ_D: (a) for $\tau_D = 0$ ms, (b) for $\tau_D = 100$ ms, (c) for $\tau_D = 200$ ms and (d) for $\tau_D = 1000$ ms. Note that ν_1 and ν_2 vary in [70,100] Hz and the colour bar represents $\Delta\nu_{ij}^c$ values.

neurons are more sensitive to changes in their external currents, which facilitates their synchronisation with neurons with similar frequencies. The more synchronised they become, the more connected they remain. Coming back to the effect of STP, we find that it decreases the influence of faster neurons on slower ones, and consequently leads to the increase of their frequency differences and to the suppress of their synchronisation. That then leads to the depression of the connectivity via STDP.

4. Effects of STP on HH neural networks with STDP

We performed a similar study for a HH neural network and analysed how the connections evolve with the combined application of STP and STDP. In particular, we start with an all-to-all (globally connected) network of $N = 100$ excitatory HH neurons. The coupling weights vary in [0,0.04] and I_i is randomly distributed so that the natural frequencies are in the range [70,100] Hz. At each time step, we check which neuron spikes and update its couplings according to the plasticity rule. We choose three initial coupling weight averages $\bar{\varepsilon}_{\text{initial}}$. The coupling matrices for the connectivity strengths ε_{ij} are shown in Fig. 7, where $\bar{\varepsilon}_{\text{initial}} = 0$ in Fig. 7(a), $\bar{\varepsilon}_{\text{initial}} = 0.01$ in Fig. 7(b) and $\bar{\varepsilon}_{\text{initial}} = 0.04$ in Fig. 7(c). For all initial conditions studied, we kept the standard deviation of $\bar{\varepsilon}_{\text{initial}}$ fixed at 0.002. In the coupling matrix (ε_{ij}), the presynaptic neurons j and postsynaptic neurons i are sorted and plotted in ascending frequency-order (i.e. from the smallest to the largest spike frequency). The final coupling matrices ε_{ij} for $\tau_D = 0$ ms are shown in Fig. 7(d), (e) and (f) for $\bar{\varepsilon}_{\text{initial}} = 0$, $\bar{\varepsilon}_{\text{initial}} = 0.01$ and $\bar{\varepsilon}_{\text{initial}} = 0.04$, respectively. In all cases, the final coupling matrices have, predominantly, connections from faster to slower spiking neurons. This behaviour was also reported in Borges et al. [20] for a neural network with STDP. Fig. 7(g), (h) and (i) present our results for $\bar{\varepsilon}_{\text{initial}} = 0$, $\bar{\varepsilon}_{\text{initial}} = 0.01$, and $\bar{\varepsilon}_{\text{initial}} = 0.04$, respectively, where $\tau_D = 100$ ms. Due to the effect of STP on the dynamics of the neurons in the network, we observe the formation of different modules of directly connected neurons. Again, the effect of STP leads to a decrease on the influence of the fastest neurons to the slowest ones, allowing for the formation of connections among those neurons with similar spike frequencies. The size of these modules increases according to the intensity of the initial coupling and their different sizes can be explained by the analysis made based on the results in Figs. 5 and 6, where the coupling shortened the frequency differences, leading to the formation of connections especially among neurons with close frequencies. This also explains why the bigger-size modules are composed of the smallest-frequency spiking neurons. Increasing τ_D to 1000 ms, leads to the disappearance of big modules and to the decrease of the number of coupled neurons, as shown in Fig. 7(j), (k) and (l). Therefore, by varying the STP recovery time τ_D, one can control the formation of modules in neural networks with STP and STDP.

We also analyse the neural in-out degree distributions of our network. Fig. 8 shows the neural in-degree (blue) and out-degree (red) distributions for $\bar{\varepsilon}_{\text{initial}} = 0.01$ with (a) $\tau_D = 0$ ms, (b) $\tau_D = 100$ ms, and (c) $\tau_D = 1000$ ms with their respective network degree probability distributions shown in panels (d), (e) and (f). We calculate the in-out degree considering the connections among neurons and not their synaptic weight. In Fig. 8(a), we observe a decrease and an increase in the in-degree and out-degree distributions, respectively, which is in accordance with the one cluster formation shown in Fig. 7(e). This configuration also exhibits a uniform in-out degree probability distribution as displayed in Fig. 8(d). In Fig. 8(b), we see

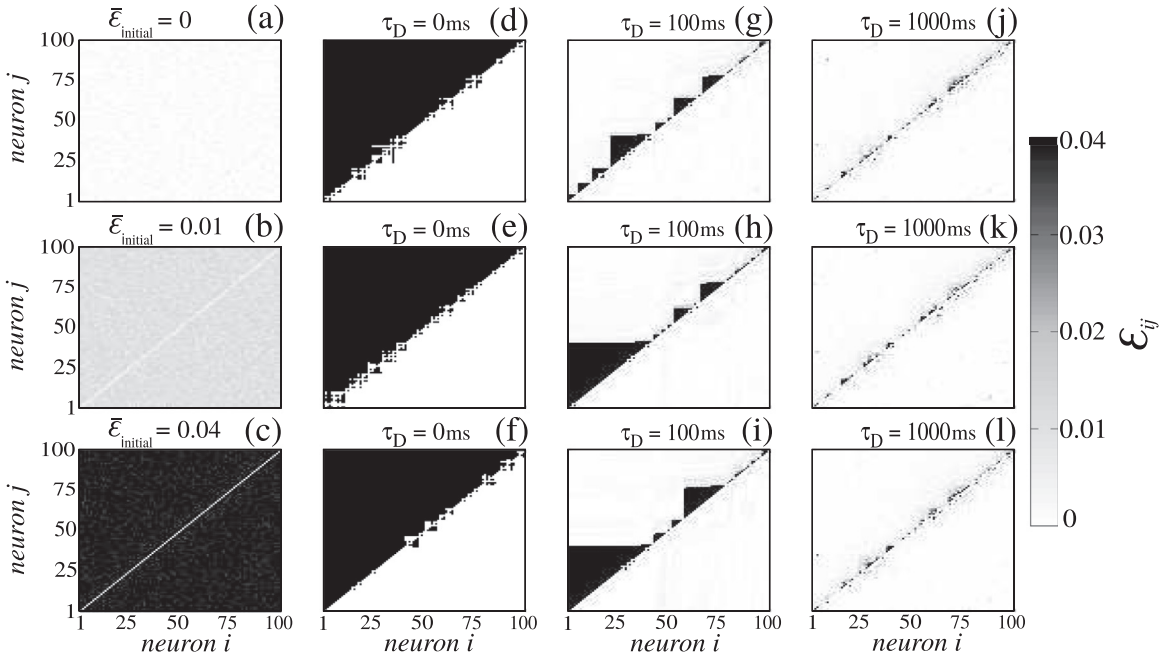

Fig. 7. The combined effect of STP and STDP on connectivity in networks of $N = 100$ excitatory coupled HH neurons and emergence of modular neural networks. The initial couplings used are: In (a) $\bar{\varepsilon}_{\text{initial}} = 0$, in (b) $\bar{\varepsilon}_{\text{initial}} = 0.01$ and in (c) $\bar{\varepsilon}_{\text{initial}} = 0.04$. We consider $\tau_D = 0$ ms for (d) $\bar{\varepsilon}_{\text{initial}} = 0$, (e) $\bar{\varepsilon}_{\text{initial}} = 0.01$ and (f) $\bar{\varepsilon}_{\text{initial}} = 0.04$. $\tau_D = 100$ ms for (g) $\bar{\varepsilon}_{\text{initial}} = 0$, (h) $\bar{\varepsilon}_{\text{initial}} = 0.01$ and (i) $\bar{\varepsilon}_{\text{initial}} = 0.04$ and $\tau_D = 1000$ ms for (j) $\bar{\varepsilon}_{\text{initial}} = 0$, (k) $\bar{\varepsilon}_{\text{initial}} = 0.01$ and (l) $\bar{\varepsilon}_{\text{initial}} = 0.04$. Note that the synaptic weights ε_{ij} (with $i, j = 1, \ldots, 100$) of the coupling matrices are encoded in grey scale in the colour bar.

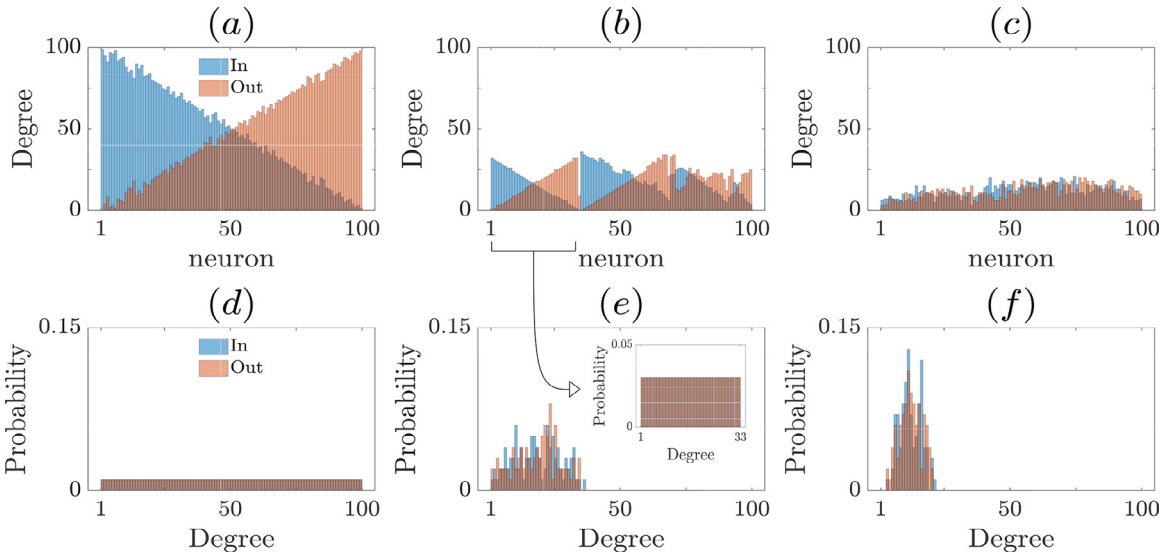

Fig. 8. Neuron in-out degree distributions for $\bar{\varepsilon}_{\text{initial}} = 0.01$ for (a) $\tau_D = 0$ ms, (b) $\tau_D = 100$ ms, and (c) $\tau_D = 1000$ ms with their respective network degree probability distributions shown in (d), (e), and (f). We calculate the in-out degree considering the connection between neurons and not the synaptic weigth.

the same neural degrees patterns restricted to the neurons within the small clusters. Fig. 8(e) shows that the network in-out degree probability distribution is similar to a Gaussian distribution, however, it does not reflect the distribution inside the clusters, as shown in the inset of Fig. 8(e). In particular, the inset displays the uniform distribution amont neurons within the first cluster. Fig. 8(c) and (f) show the degree and probability, respectively, the results for the in-degree is similar to the out-degree. The decrease in both degrees is expected as the network becomes sparse for higher τ_D.

To study further the observed modules, we consider connections with $\varepsilon_{ij} > 0.002$ (i.e. with connectivity strength bigger than 5% of the maximal coupling strength). Thus, weaker connections are not considered in the resulting network analysis.

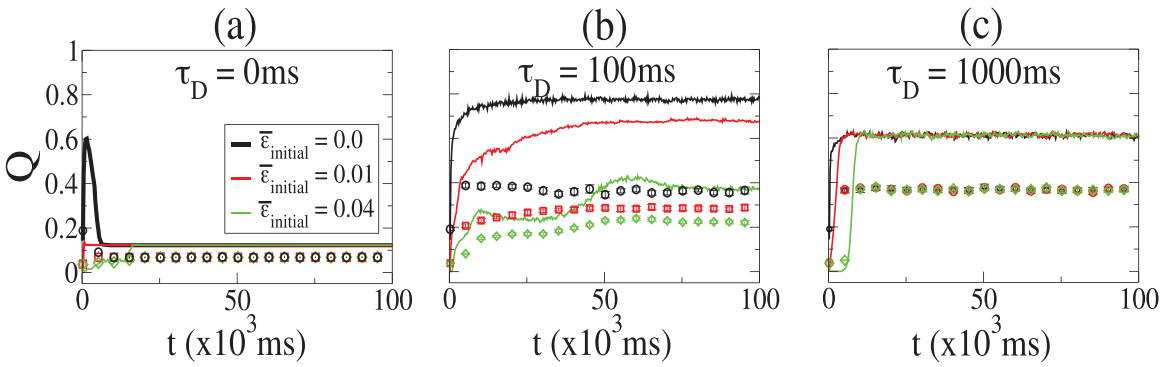

Fig. 9. Time evolution of modularity Q for (a) $\tau_D = 0$ ms, (b) $\tau_D = 100$ ms and (c) $\tau_D = 1000$ ms. Q was calculated over the time evolution of the coupling matrix and the coloured curves represent the network average initial coupling: the black curve is for $\bar{\varepsilon}_{\text{initial}} = 0$, the red for $\bar{\varepsilon}_{\text{initial}} = 0.01$ and the green for $\bar{\varepsilon}_{\text{initial}} = 0.04$. The coloured symbols represent the average Q for random networks computed by rewiring the connections in the corresponding original networks. For example, the black symbols represent the average Q calculated over 20 random networks generated by rewiring randomly the connections in the original networks (black curve).

This procedure also avoids measurement errors that might be caused by connections whose weights fluctuate closely to zero over time.

To evaluate how modular structures evolve over time, we compute the modularity Q by using the Louvain method [55]. Q is measured across network partitions in densely connected communities. In particular, the modularity assumes values in the range $[-1, 1]$ comparing the density of connections within communities with the density among communities. The best network partition in modules is one that maximises modularity. Q is defined as [56]

$$Q = \frac{1}{W}\sum_{i}^{N}\sum_{j}^{N}\left(\varepsilon_{i,j} - \frac{\omega_i\omega_j}{W}\right)\delta(c_i, c_j), \tag{14}$$

where $\omega_i = \sum_j^N \varepsilon_{ij}$ is the sum of the connection weights received by node i and $W = \sum_i^N \sum_j^N \varepsilon_{ij}$ the sum of all weights in the coupling matrix. The term c_i represents the community that neuron i has been allocated to and $\delta(c_i, c_j)$ is given by

$$\delta(c_i, c_j) = \begin{cases} 1, & \text{if } c_i = c_j, \\ 0, & \text{otherwise.} \end{cases} \tag{15}$$

The Louvain [55] method is defined in two steps: At first, each node in the network is considered as a community in itself, and thus initially, there will be as many communities as nodes in the network. At this stage, each node i is reassigned to the community of each of its neighbours j, then i will be permanently fixed in the community that promotes the largest gain in modularity Q (positive gain). This process is applied repeatedly to all network nodes until there are no more gains in Q. The second step amounts to taking the defined communities at the end of the first step and consider them as the nodes of a new network. The weight of the connections between these new nodes is given by the sum of the weights of the connections between the nodes present in the communities (defined in the first step). Once the new network is computed, the first step can be applied again to its nodes. This process occurs repeatedly until no further changes to Q occur and a maximum value is thus obtained.

Fig. 9 shows the time evolution of modularity Q for the three recovery times, $\tau_D = 0$ ms, $\tau_D = 100$ ms and $\tau_D = 1000$ ms. The colours represent the initial connectivity strengths in the coupling matrix: the black curve is for $\bar{\varepsilon}_{\text{initial}} = 0$, the red curve for $\bar{\varepsilon}_{\text{initial}} = 0.01$ and the green curve for $\bar{\varepsilon}_{\text{initial}} = 0.04$. The coloured symbols represent the average Q values calculated over 20 random networks obtained by rewiring all connections of the original networks. We did this to compare our results with those obtained for random networks with the same connections and number of nodes (which we call random variants). Unless stated otherwise, the symbols in Fig. 9 represent the measurements taken on the random variants.

In Fig. 9(a), we observe that for $\tau_D = 0$ ms (instantaneous recovery), Q is very low for all $\bar{\varepsilon}_{\text{initial}}$ connectivity strengths, remaining constant after a small transient. These results confirm those in Fig. 7(d), (e) and (f). In Fig. 9(b) for $\tau_D = 100$ ms, Q assumes its largest value for $\bar{\varepsilon}_{\text{initial}} = 0$, confirming what we observed in Fig. 7(g), (h) and (i) by comparing the number of modules. It is also apparent that Q stabilises for simulation times t greater than 80000 ms as there are no changes in the modular structures occurring in the networks anymore. Interestingly, Fig. 9(c) shows that for $\tau_D = 1000$ ms, Q converges to the same value (i.e. $Q \approx 0.6$) for all $\bar{\varepsilon}_{\text{initial}}$ coupling strengths, again in accordance with the results in Fig. 7(j), (k), (l), which show networks with similar configurations regardless of the initial coupling. Finally, in all cases considered, we find that the modularity of the networks is bigger than their random variants.

Next, we compute other quantities that characterise the structure of the networks considered previously, such as the mean path-length, clustering coefficient and assortativity. In particular, a path is defined as the route that passes through network connections, connecting nodes i and j. The path with the shortest number of connections is called the shortest path

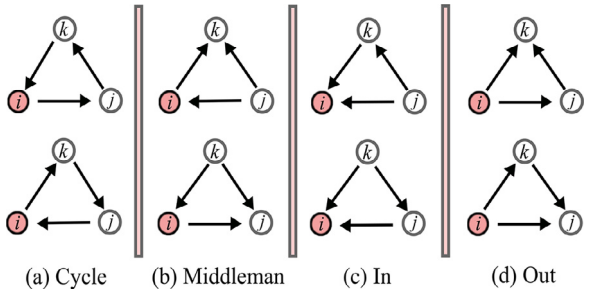

Fig. 10. The 8 distinct triangular motifs in directed networks. The motifs are considered with respect to node i depicted in red and are split into the cycle, middleman, and in out motifs. (For interpretation of the references to color in this figure legend, the reader is referred to the web version of this article.)

l_{ij} [57]. The networks we consider here are directed, so l_{ij} is not necessarily equal to l_{ji}. In general, the shortest average path length is given by

$$\bar{L} = \frac{1}{N(N-1)} \sum_{i}^{N} \sum_{j \neq i}^{N} l_{ij}, \tag{16}$$

where N is the number of nodes in the network. In our approach, we calculated $\bar{L}$ via a breadth-first search approach [57] and do not consider the weights of the connections. If there is no possible directed path l_{ij} between nodes i and j, then it is not considered in the calculations in Eq. (16).

The second quantity considered is the clustering coefficient CC_i, which measures the degree to which the neighbours of a node i are connected to each other and varies in [0,1]. It is computed by considering the number of triangular motifs made by node i and its neighbours compared to all possible triangular motifs of that node [57]. For directed networks, given 3 connected nodes i, j and h, there are 8 distinct triangular motifs, shown in Fig. 10. These motifs are further organised into 4 groups when considering node i as the reference node: Fig. 10(a) shows a "cycle" motif, Fig. 10(b) a "middleman" motif, Fig. 10(c) an "in" motif and Fig. 10(d) an "out" motif. For each motif, we calculate $CC_i^{(\mathrm{cyc,mid,in,out})}$ relative to node i, as shown in [58].

For directed and weighted networks, there are 4 types of clustering coefficients

$$\begin{aligned}
CC_i^{\mathrm{cyc}} &= \frac{\frac{1}{2}\sum_j^N \sum_h^N \left[\varepsilon_{ij}^{1/3}\varepsilon_{jh}^{1/3}\varepsilon_{hi}^{1/3} + \varepsilon_{ih}^{1/3}\varepsilon_{hj}^{1/3}\varepsilon_{ji}^{1/3}\right]}{d_i^{\mathrm{in}} d_i^{\mathrm{out}} - d_i^{\leftrightarrow}}, \\
CC_i^{\mathrm{mid}} &= \frac{\frac{1}{2}\sum_j^N \sum_h^N \left[\varepsilon_{ih}^{1/3}\varepsilon_{jh}^{1/3}\varepsilon_{ji}^{1/3} + \varepsilon_{ij}^{1/3}\varepsilon_{hi}^{1/3}\varepsilon_{hj}^{1/3}\right]}{d_i^{\mathrm{in}} d_i^{\mathrm{out}} - d_i^{\leftrightarrow}}, \\
CC_i^{\mathrm{in}} &= \frac{\frac{1}{2}\sum_j^N \sum_h^N \left[\varepsilon_{ij}^{1/3}\varepsilon_{ih}^{1/3}\varepsilon_{jh}^{1/3} + \varepsilon_{ij}^{1/3}\varepsilon_{ih}^{1/3}\varepsilon_{hj}^{1/3}\right]}{d_i^{\mathrm{in}}(d_i^{\mathrm{in}} - 1)}, \\
CC_i^{\mathrm{out}} &= \frac{\frac{1}{2}\sum_j^N \sum_h^N \left[\varepsilon_{hi}^{1/3}\varepsilon_{ji}^{1/3}\varepsilon_{jh}^{1/3} + \varepsilon_{hi}^{1/3}\varepsilon_{ji}^{1/3}\varepsilon_{hj}^{1/3}\right]}{d_i^{\mathrm{out}}(d_i^{\mathrm{out}} - 1)},
\end{aligned} \tag{17}$$

where $d_i^{\mathrm{in}} = \sum_j^N a_{ij}$ is the in-degree of node i and $d_i^{\mathrm{out}} = \sum_j^N a_{ji}$ its out-degree. The term $d_i^{\leftrightarrow} = \sum_j^N a_{ij}a_{ji}$ represents the number of bilateral connections between node i and its neighbours. For the calculation of d_i^{in}, d_i^{out} and $d_i^{\leftrightarrow}$, the coupling weights are not considered, only the number of connections, that is $a_{ij} = 1$ if $\varepsilon_{ij} > 0.002$, otherwise $a_{ij} = 0$.

Consequently, the clustering coefficient of the network, CC^*, is calculated by averaging CC_i^* over all N nodes in the network

$$CC^* = \frac{1}{N}\sum_i^N CC_i^*, \tag{18}$$

where $*$ stands for either of the cyc, mid, in or out motifs.

The last quantity considered in our study is assortativity, which is the correlation coefficient (i.e. the Pearson correlation [59]) between the degrees of nodes on two opposite ends of a connection in a network, for all connections in the network. This correlation varies in $[-1, 1]$ and, is positive in assortative networks and negative in disassortative networks. Since our networks are directed and weighted, we use the four directed assortativity measures defined in [60].

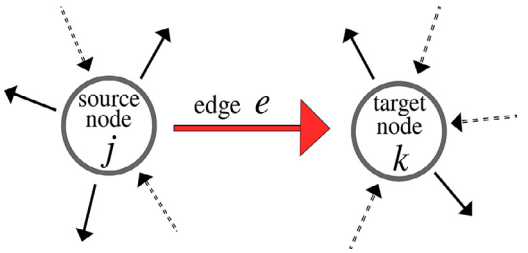

Fig. 11. Representative illustration of an edge e and, the source j and target k nodes considered in Eq. (19).

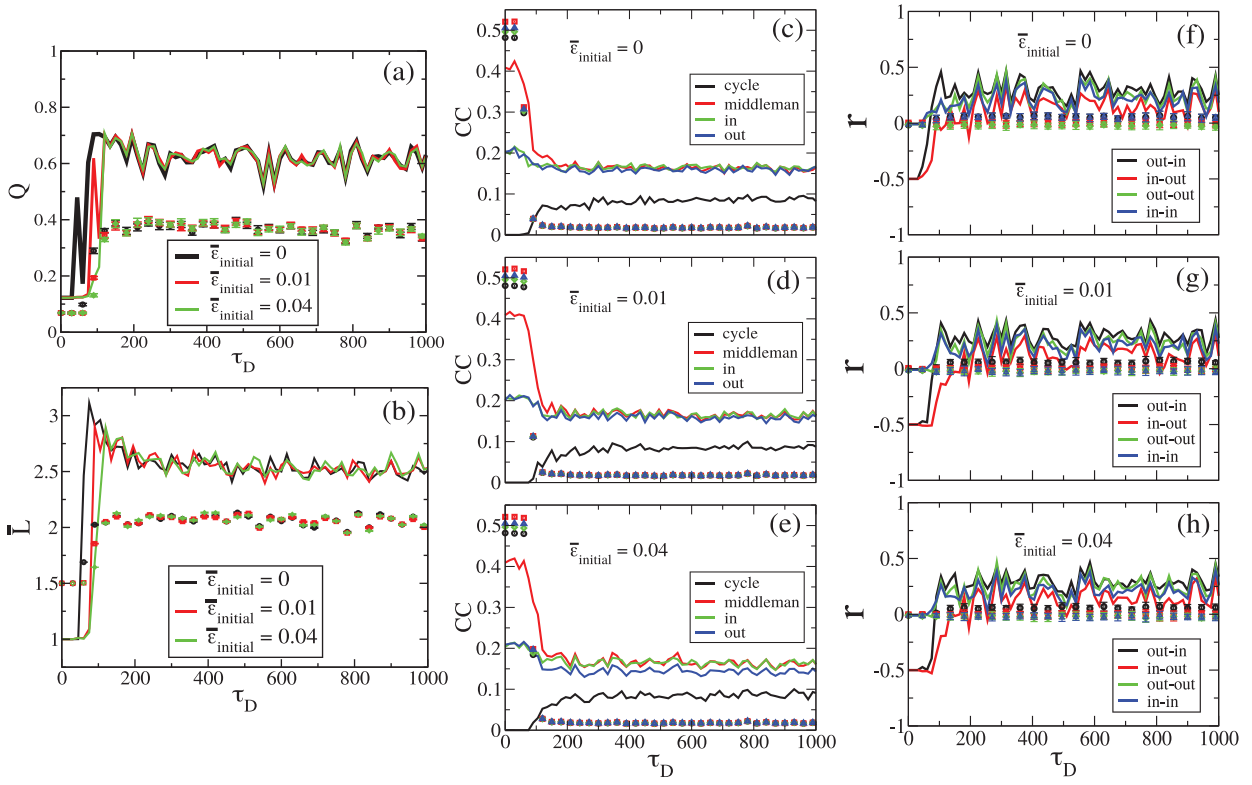

Fig. 12. Structural properties of the final coupling matrix configuration (coloured curves) and their respective random variants (averaged over 20 random networks, coloured symbols) as a function of the recovery time τ_D. Panels (a) and (b) show the modularity Q and average shortest path length $\bar{L}$ for three different average initial couplings: $\bar{\varepsilon}_{\text{initial}} = 0$ in black, $\bar{\varepsilon}_{\text{initial}} = 0.01$ in red and $\bar{\varepsilon}_{\text{initial}} = 0.04$ in green. In (c), (d) and (e), we show all clustering coefficients for $\bar{\varepsilon}_{\text{initial}} = 0$, $\bar{\varepsilon}_{\text{initial}} = 0.01$, and $\bar{\varepsilon}_{\text{initial}} = 0.04$, respectively. Panels (f), (g) and (h) show the assortativity r for $\bar{\varepsilon}_{\text{initial}} = 0$, $\bar{\varepsilon}_{\text{initial}} = 0.01$, and $\bar{\varepsilon}_{\text{initial}} = 0.04$, respectively.

In particular, let a and b be indices representing the type of degree (i.e. in- and out-degree) and j_e^a and k_e^b the a- and b-degree from source node j to target node k of an edge e. Fig. 11 shows an illustrative representation of edge e and their respective source nodes j and target nodes k. Foster et al. [60] defined the assortativity measure $r(a,b)$ as

$$r(a,b) = \frac{N_e^{-1}\sum_e^{N_e}\left[(j_e^a - \bar{j}^a)(k_e^b - \bar{k}^b)\right]}{\sigma^a \sigma^b}, \tag{19}$$

where N_e is the number of edges in the network, $\bar{j}^a = N_e^{-1}\sum_e^{N_e} j_e^a$ the average in- and out-degrees of the source node and $\sigma^a = \sqrt{N_e^{-1}\sum_e^{N_e}(j_e^a - \bar{j}^a)^2}$ its deviation, calculated for all edges. The equations for $\bar{k}^b$ and σ^b are similarly defined. In our approach, instead of in- and out-degrees, we use the in- and out-strength from the source and target nodes, given by the sum of their in- and out-coupling weights. A positive assortativity coefficient indicates that nodes tend to connect to other nodes with the same or similar strength.

Fig. 12 shows the results of the computations of the quantities discussed previously as a function of τ_D in [0,1000] ms. In all computations, we consider the final coupling matrix obtained after $t = 200000$ ms of simulated data. Fig. 12(a) shows the modularity Q for 3 initial couplings: $\bar{\varepsilon}_{\text{initial}} = 0$ in black, $\bar{\varepsilon}_{\text{initial}} = 0.01$ in red and, $\bar{\varepsilon}_{\text{initial}} = 0.04$ in green and their random

variants given by different symbols with their respective colours. We note that for $\tau_D \lessapprox 30$ ms and for all 3 $\bar{\varepsilon}_{\text{initial}}$ values, Q is low. For $30\,\text{ms} < \tau_D \lessapprox 120$ ms, Q depends on $\bar{\varepsilon}_{\text{initial}}$. In particular, the lower the initial average coupling $\bar{\varepsilon}_{\text{initial}}$, the more modular the final configuration of the network. For $\tau_D \gtrapprox 120$ ms, there is no dependence on $\bar{\varepsilon}_{\text{initial}}$ and the resulting networks exhibit similar modularity values. In all cases of $\bar{\varepsilon}_{\text{initial}}$, Q is higher than that calculated for their random variants, which shows that the resulting networks do not have characteristics of random networks.

Fig. 12 (b) shows the results for the average path length $\bar{L}$ for the same three $\bar{\varepsilon}_{\text{initial}}$ values. For $\tau_D < 30$ ms, the average path $\bar{L} = 1$, in accordance with Fig. 7(d), (e) and (f), where we observe a network where all nodes are connected to all other nodes with unidirectional connections. For $30\,\text{ms} < \tau_D < 120$ ms, the average path length $\bar{L}$ is bigger for weaker initial couplings. This is because weak initial couplings result in the formation of a larger number of modular structures (as seen in Fig. 12(a)), which results in a greater path for one node to access other nodes in different modules, possibly crossing through other modules. For $\tau_D > 120$ ms, we see that $\bar{L} \approx 2.5$ for all 3 $\bar{\varepsilon}_{\text{initial}}$ values. In contrast, the average path lengths $\bar{L}$ for the random variants are smaller than those for the original networks.

Fig. 12 (c), (d) and (e) present the 4 types of clustering coefficients for $\bar{\varepsilon}_{\text{initial}} = 0$, $\bar{\varepsilon}_{\text{initial}} = 0.01$ and $\bar{\varepsilon}_{\text{initial}} = 0.04$. The black curve represents CC^{cyc}, the red CC^{mid}, the green CC^{in} and the blue CC^{out}. In all cases, the results are similar. It is worth it to note that for $\tau_D < 120$ ms, CC^{mid} has the highest value and CC^{cyc} the lowest. These results build on what we have already observed: the action of STDP promotes connections from faster to slower spiking neurons and do not permit cyclic connections (see Fig. 10(a)). As τ_D increases, CC^{mid} converges to $\text{CC}^{\text{in}}, \text{CC}^{\text{out}} \approx 0.15$ and CC^{cyc} increases to about 0.09. For the random variants of the networks (coloured symbols), we see that for $\tau_D < 120$ ms, all clustering coefficients are similar and larger than those for the original networks. This is because for such τ_D values, the networks from which they were generated (Fig. 7(d), (e), (f)) are densely connected and the high number of connections allows for the formation of triangular motifs without any of the 4 types occurring preferentially. For $\tau_D > 120$, all random networks have their clustering coefficients fluctuate near zero. In this case, the generating networks are more sparse (as in Fig. 7(g), (h), (i)), which makes their random variants have low probability in forming triangular motifs. We note that these clustering coefficients are not high enough to claim with certainty that the networks have a small-world topology.

The right column of plots in Fig. 12 shows the 4 assortativity measures, r, computed for the considered networks with $\bar{\varepsilon}_{\text{initial}} = 0$, $\bar{\varepsilon}_{\text{initial}} = 0.01$, and $\bar{\varepsilon}_{\text{initial}} = 0.04$. The black curves represent the out-strength/in-strength correlation $r(\text{out}, \text{in})$ between the source and target nodes, the red curve the in-strength/out-strength correlation $r(\text{in}, \text{out})$, the green curve the out-strength/out-strength correlation $r(\text{out}, \text{out})$ and the blue curve, the in-strength/in-strength correlation $r(\text{in}, \text{in})$.

In Fig. 12(f), (g), (h) and for the three $\bar{\varepsilon}_{\text{initial}}$ values, we find that for $\tau_D < 100$ ms, the networks are disassortative as $r(\text{out}, \text{in})$ and $r(\text{in}, \text{out})$ are negative and, at the same time, neither assortative nor disassortative as $r(\text{out}, \text{out})$ and $r(\text{in}, \text{in})$ are approximately equal to 0. The predominance of the connections from the fastest to the slowest neurons is responsible for the disassortative properties of the network. Neurons that receive many strong connections (the slowest ones) generally do not send connections to neurons that also send many strong connections (the fastest ones). The values of $r(\text{out}, \text{out})$ and $r(\text{in}, \text{in})$ are low due to the fact there are no neurons that send (receive) many strong connections connected with other neurons that send (receive) many strong connections. As τ_D increases, all correlations grow, being mostly positive with $r(\text{out}, \text{in})$ being the largest. This shows a greater correlation in the network of high out-strength nodes to connect with nodes with high in-strength and corroborates the results in Fig. 7, where connections occur preferably from the faster neurons (which have a high out-strength) to the slower ones (with high in-strength). For the random variants of these networks, all correlations are close to zero for the entire τ_D range, a result completely different to those for the original networks. We thus conclude that the original networks are far from being purely random networks, exhibiting a type of preferential attachment in their connectivities.

In the analysis of the structural properties of the networks, the topology may vary greatly depending on τ_D. In all cases studied, the networks were different from random or small-world networks, since the average path lengths are bigger than in random networks and their clustering coefficients are small than in random networks. This corroborates further the results obtained previously here that there is a complex process taking place in which modules are formed via preferential attachment.

5. Conclusions

In this paper, we studied the effects of plasticity (STP and STDP) on networks of excitatory coupled Hodgkin-Huxley neurons. Neural plasticity is responsible for alterations in the organisation and structure of the brain, and both play an important role in synaptic weights. Besides, STDP has a longer time scale than STP, so it affects differently the structure and function in brain networks.

We started analysing the effect of STP in a pair of neurons that are initially, either uncoupled or bidirectionally coupled. For initially uncoupled neurons, the action of STP and STDP promotes directed connections among neurons with small spike frequency differences, from the faster to the slower spiking neurons. The increase of the recovery-time shortened the interval of frequency differences where connections are formed. When neurons are initially coupled, their frequency difference is smaller and increases the size of the area of directed connections. We found that STP induces uncoupling, depending on the recovery time: the bigger the recovery time, the smaller the interval of frequency difference that allows for the formation of connections.

Next, we build a neural network with an all-to-all topology. Considering only STDP, the coupling matrix exhibits directed connections from neurons with high to neurons with low spike frequencies. We have shown that due to STP, neural networks equipped with STDP facilitate the formation of synapses among neurons with similar spike frequencies only and that modular neural networks can emerge as a direct result of the combined effect of STP and STDP, a phenomenal structure also depicted by neurophysiological and experimental studies. However, by increasing the STP recovery time, the number of connections decreased and as a consequence, the modules disappeared. That is actually a way to control the modular organisation in neural networks. The structure of these modular networks is complex, unlike those in random or small-world networks, resembling more to networks with preferential attachment properties.

In future, we plan to study neural networks with greater diversity in chemical synapses, addressing other STP and STDP rules related to synapses between excitatory-inhibitory and inhibitory-inhibitory neurons [54]. Finally, another interesting aspect of our work would be the introduction of time delay in the synaptic transmission to study how it affects the evolution of the couplings and the modular properties of neural networks.

Declaration of Competing Interest

We wish to confirm that there are no known conflicts of interest associated with this work and there has been no significant financial support for this work that could have influenced its outcome.

No conflict of interest exists.

Acknowledgements

We wish to acknowledge Dr Serhiy Yanchuk for the valuable suggestions and remarks. The support offered by the International Visiting Fellowships Scheme of the University of Essex, CNPq, CAPES, Fundação Araucária and São Paulo Research Foundation (processes FAPESP 2011/19296-1, 2015/ 07311-7, 2016/23398-8, 2017/13502-5, 2017/18977-1, 2017/20920-8, 2020/ 04624-2). The research was also supported by the 2015/50122-0 São Paulo Research Foundation (FAPESP) and DFG-IRTG 1740/2 grants.

References

[1] Tewari SG, Gottipati MK, Parpura V. Mathematical modeling in neuroscience: neural activity and its modulation by astrocytes. Front Integr Neurosci 2016;10:3.
[2] Lapicque L. Recherches quantitatives sur l'excitation electrique des nerfs traitée comme une polarization. J Physiol Pathol Gen 1907;9:620–35.
[3] Hodgkin AL, Huxley AF. A quantitative description of membrane current and its application to conduction and excitation in nerve. J Physiol 1952;117:500–44.
[4] Zhu Z, Wang R, Zhu F. The energy coding of a structural neural network based on the Hodgkin-Huxley model. Front Neurosci 2018;12:122.
[5] Protachevicz PR, Borges FS, Lameu EL, Ji P, Iarosz KC, Kihara AH, Caldas IL, Szezech JD, Baptista MS, EEN M, ChG A, Batista AM, Kurths J. Bistable firing pattern in a neural network model. Front Comput Neurosc 2019;13:19.
[6] Viana RL, Borges FS, Iarosz KC, Batista AM, Lopes SR, Caldas IL. Dynamic range in a neuron network with electrical and chemical synapses. Commun Nonlinear Sci Numer Simul 2014;19:164–72.
[7] CAS B, Viana RL, Lopes SR, Batista AM. Dynamic range in small-world networks of Hodgkin-Huxley neurons with chemical synapses. Physica A 2014;410:628–40.
[8] Borges FS, Lameu EL, Batista AM, Iarosz KC, Baptista MS, Viana RL. Complementary action of chemical and electrical synapses to perception. Physica A 2015;430:236–41.
[9] Antonopoulos C. Dynamic range in the C.elegans brain network. Chaos 2016;26:1054–500.
[10] Hizanidis J, Kouvaris NE, Zamora-López G, Díaz-Guilera A, ChG A-p. Chimera-like states in modular neural networks. Sci Rep 2016;6:19845.
[11] Borges FS, Protachevicz PR, Lameu EL, Boneti RC, Iarosz KC, Caldas IL, Baptista MS, Batista AM. Synchronised fire patterns in a random network of adaptive exponential integrate-and-fire neuron model. Neural Netw 2017;90:1–7.
[12] Protachevicz PR, Borges RR, Borges FS, Iarosz KC, Caldas IL, Lameu EL, EEN M, Viana RL, Sokolov IM, FAS F, Kurths J, Batista AM, C-Y L, He Y, C-P L. Synchronous behaviour in network model based on human cortico-cortical connections. Physiol Meas 2018;39:074006.
[13] Lameu EL, Yanchuk S, EEN M, Borges FS, Iarosz KC, Caldas IL, Protachevicz PR, Borges RR, Viana RL, Szezech JD, Batista AM, Kurths J. Recurrence quantification analysis for the identification of burst phase synchronization. Chaos 2018;28:085701.
[14] ChG A, Martinez-Bianco E, Baptista MS. Evaluating performance of neural codes in model neural communication networks. Neural Netw 2019;109:90–102.
[15] ChG A, Srivastava S, SEDS P, Baptista MS. Do brain networks evolve by maximizing their information flow capacity? PLOS Comput Biol 2015;11(8):e1004372.
[16] ChG A, Fokas AS, Bountis TC. Dynamical complexity in the C.elegans neural network. Eur Phys J 2016;225:1255–69.
[17] Borges FS, Lameu EL, Iarosz KC, Protachevicz PR, Caldas IL, Viana RL, EEN M, Batista AM, Baptista MS. Inference of topology and the nature of synapses, and the flow of information in neural networks. Phys Rev E 2018;97:022303.
[18] Romani S, Tsodyks M. Short-term plasticity based network model of place cells dynamics. Hippocampus 2015;25:94–105.
[19] Zenke F, Agnes EJ, Gerstner W. Diverse synaptic plasticity mechanisms orchestrated to form and retrieve memories in spiking neural networks. Nat Commun 2015;6:6922.
[20] Borges RR, Borges FS, Lameu EL, Batista AM, Iarosz KC, Caldas IL, et al. Spike-timing-dependent plasticity induces non-trivial topology in the brain. Neural Netw 2017;88:58–64.
[21] Burke SN, Barnes CA. Neural plasticity in the ageing brain. Nat Rev Neurosci 2006;7:30–40.
[22] Berlucchi G. Neural plasticity: historical roots and evolution of meaning. Exp Brain Res 2009;192:307–19.
[23] James W. The principles of psychology. Chapter IV Habits; 1890.
[24] Stahnisch FW, Nitsch R. Santiago Ramón y Cajal's concept of neural plasticity: the ambiguity lives on. Trends Neurosci 2002;25:589–91.
[25] Lashley KS. Studies of cerebral function in learning. VI. The theory that synaptic resistance is reduced by the passage of the nerve impulse. Psychol Rev 1924;31:369–75.
[26] Konorski J. Conditioned reflexes and neuron organization. Cambridge: Cambridge University Press; 1948.
[27] Hebb DO. The organization of behaviour. A neuropsychological theory. New York: Wiley; 1949.

[28] Bennett EL, Diamond MC, Krech D, Rosenzweig MR. Chemical and anatomical plasticity of the brain. Science 1964;146:610–19.
[29] Lameu EL, EEN M, Borges FS, Iarosz KC, Caldas IL, Borges RR, Protachevicz PR, Viana RL, Batista AM. Alterations in brain connectivity due to plasticity and synaptic delay. Eur Phys J Spec Top 2018;227:673–82.
[30] Rangaraju V, Lauterbach M, Schuman EM. Spatially stable mitochondrial compartments fuel local translation during plasticity. Cell 2019;176:73–84.
[31] Abbott LF, Nelson SB. Synaptic plasticity: taming the beast. Nat Neurosci 2000;3:1178–83.
[32] Borges RR, Borges FS, Lameu EL, Protachevicz PR, Iarosz KC, Caldas IL, Viana RL, EEN M, Baptista MS, Grebogi C, Batista AM. Synaptic plasticity and spike synchronization in neural networks. Braz J Phys 2017;47:678–88.
[33] McDonnell MD, Graham BP. Phase changes in neural postsynaptic spiking due to short term plasticity. PLoS Comput Biol 2017;13:e1005634.
[34] Asl MM, Valizadeh A, Tass PA. Delay-induced multistability and loop formation in neuronal networks with spike-timing-dependent plasticity. Sci Rep 2018;8:12068.
[35] Markram H, Gerstner W, Sjöström PJ. Spike-timing-dependent plasticity: a comprehensive overview. Front Synaptic Neurosci 2012;4:1–3.
[36] Borges RR, Borges FS, Lameu EL, Batista AM, Iarosz KC, Caldas IL, Viana RL, MAF S. Effects of the spike timing-dependent plasticity on the synchronization in a random Hodgkin-Huxley neural network. Commun Nonlinear Sci Numer Simulat 2016;34:12–22.
[37] Clopath C, Büsing L, Vasilaki E, Gerstner W. Connectivity reflects coding: a model of voltage-based STDP with homeostasis. Nat Neurosci 2010;13:344–52.
[38] Tass PA, Popovych OV. Unlearning tinnitus-related cerebral synchrony with acoustic coordinated reset stimulation: theoretical concept and modelling. Biol Cybern 2012;106:27–36.
[39] Popovych OV, Yanchuk S, Tass PA. Self-organized noise resistance of oscillatory neural networks with spike-timing-dependent plasticity. Sci Rep 2013;3:2926.
[40] Lücken L, Popovych OV, Tass PA, Yanchuk S. Noise-enhanced coupling between two oscillators with long-term plasticity. Phys Rev E 2016;93:32210.
[41] Gerstner W, Kempter R, van Hemmen JL, Wagner H. A neuronal learning rule for sub-millisecond temporal coding. Nature 1996;383:76–8.
[42] Stevens CF, Wang Y. Facilitation and depression at single central synapses. Neuron 1995;14:795–802.
[43] Abbott LF, Varela JA, Sen K, Nelson SB. Synaptic depression and cortical gain control. Science 1997;275:220–4.
[44] Zucker RS, Regehr WG. Short-term synaptic plasticity. Annu Rev Physiol 2002;64:355–405.
[45] Hennig MH. Theoretical model of synaptic short term plasticity. Front Comput Neurosci 2013;7:45.
[46] Itskov V, Hansel D, Tsodyks M. Short-term facilitation may stabilize parametric working memory trace. Front Comput Neurosci 2011;5:40.
[47] York LC, van Rossum M. Recurrent networks with short term synaptic depression. J Comp Neurosci 2009;27:607–20.
[48] Bi GQ, Poo MM. Synaptic modifications in cultured hippocampal neurons: dependence on spike timing, synaptic strength, and postsynaptic cell type. J Neurosci 1998;18:10464–72.
[49] Bi GQ, Poo MM. Synaptic modification by correlated activity: Hebb's postulate revisited. Annu Rev Neurosci 2001;24:139–66.
[50] Liu S-C. Analog VLSI circuits for short-term dynamic synapses. EUR ASIP J Appl Signal Process 2003;7:620–8.
[51] Zucker RS. Short-term synaptic plasticity. Ann Rev Neurosci 1989;12:13–31.
[52] Nicolini C, Bifone A. Modular structure of brain functional networks: breaking the resolution limit by surprise. Sci Rep 2016;6:19250.
[53] Sporns O, Betzel RF. Modular brain networks. Annu Rev Psychol 2016;67:613–40.
[54] Caporale N, Dan Y. Spike timing-dependent plasticity: a Hebbian learning rule. Annu Rev Neurosci 2008;31:25–46.
[55] Blondel VD, Guillaume J, Lambiotte R, Lefebvre E. Fast unfolding of communities in large networks. J Stat Mech 2008;8:P10008.
[56] MEJ N. Analysis of weighted networks. Phys Rev E 2004;70:056131.
[57] Barabási A, Pósfai M. Network science. Cambridge: Cambridge University Press; 2016.
[58] Fagiolo G. Clustering in complex directed networks. Phys Rev E 2007;76:026107.
[59] MEJ N. Assortative mixing in networks. Phys Rev Lett 2002;89:208701.
[60] Foster JG, Foster DV, Grassberger P, Paczuski M. Edge direction and the structure of networks. PNAS 2010;107:10815–20.